

Short Communication

Preparation of Nitrogen Doped Carbon Nanofibers for Electrochemical Determination of Cd(II) and Pb(II) Ions

Shupeng Liu and Xiaowei Zhang*

HeBei GEO University (School of Gemology and Material), Shijiazhuang, 050031, Hebei, China

*E-mail: zhangxiaowei@hgu.edu.cn

Received: 7 June 2020 / Accepted: 11 August 2020 / Published: 31 August 2020

It is very important to detect heavy metal ions in coal mine wastewater. In this work, we developed a simple electrospinning and carbonization method to prepare nitrogen-doped carbon nanofibres based on ZIF-8 metal-organic nanoparticles. ZIF-8/polyacrylonitrile was prepared by electrospinning and then heat-treated in a nitrogen atmosphere. Then, the obtained material was treated with hydrochloric acid to remove residual zinc impurities. Carbon nanofibres were prepared and applied to modify the surface of an electrode for the electrochemical detection of Cd(II) and Pb(II). According to the experimental results, glassy carbon electrodes modified with nitrogen-doped carbon nanofibres showed good linear correlation, and the detection limits were 1.11 µg/L and 0.72 µg/L for Cd(II) and Pb(II) ions, respectively.

Keywords: Heavy metal; Electrochemistry; Nitrogen-doped porous carbon nanofibers; Sensor; Electrode modification

1. INTRODUCTION

Heavy metal ions have a strong toxicity and stability, are difficult to degrade in natural environments and can be transmitted through the food chain [1–4]. Even in the case of very low concentrations, they can cause serious damage to the human body. In particular, the heavy metal elements discharged from the chemical industry, mining industry and metallurgy industry have large impacts on natural organisms once they enter a water body [5,6]. With the exploitation and utilization of various minerals, a large number of heavy metal elements are discharged from wastewater or polluted water from the chemical industry, machinery, coal mining and other industrial production. They are widely distributed in the water source soil, causing great pollution and harm to the environment [7–9].

Coal is a type of combustible ore, formed by long-term physical and chemical action and buried underground under the action of geological movement [10–13]. In the process of coal formation, coal is mixed with other ores to form a complex aggregate. Most of these ores are nonflammable metal and

nonmetal ores. Coal ash is formed when coal is used for thermal power generation and heating. Nonflammable metal ore elements are concentrated in coal ash, including some heavy metal elements. In the process of coal-washing and processing, a large amount of circulating water is used [14–16]. After the washing process, the circulating water may contain a small amount of lead and cadmium, which can enter the natural environment and pollute water sources. After being absorbed by plants and fish, polluted water can enter the human body through the food chain. If people drink the polluted water directly, it accumulates in the human body. After a long period of accumulation, Cd(II) and Pb(II) ions in the human body start to accumulate in organs, leading to organ cancer [17–19].

At present, methods to detect Cd(II) and Pb(II) in water mainly include atomic absorption spectrometry (AAS), atomic fluorescence spectrometry (AFS), inductively coupled plasma atomic emission spectrometry (ICP-MS) and electrochemical methods [20–25]. The spectral methods are expensive and complex to operate because these large-scale instruments are not easy to carry. Therefore, they are only suitable for laboratory analysis of heavy metals, which limits the application and development of field detection [26–28]. However, compared with spectroscopic methods, electrochemical methods have the advantages of high sensitivity, low equipment price, easy operation and real-time monitoring and are suitable for all levels of heavy metal detection. Moreover, considering that the wastewater from coal preparation plants and the polluted water from lead-zinc mines are located in regions with relatively high poverty, the electrochemical method is a very suitable platform to monitor the content of heavy metal ions in wastewater in real time.

Carbon materials doped with nitrogen and sulphur can provide excellent sensitivity and selectivity for heavy metal detection [29]. The porous structures formed by nitrogen and carbon materials can improve the electrochemical-sensing performance. In addition, this type of structure provides a large number of porous sites for the adsorption of heavy metals [30,31]. Nitrogen can be pyrolyzed by in situ pyrolysis of nitrogen-containing precursors, such as polyvinylpyrrolidone, melamine or ZIF-8. Carbon nanofibres have attracted much attention due to their excellent structural stiffness and affinity for heavy metals. Electrospinning is considered a simple and effective technique for the preparation of carbon nanofibres. In this work, we developed a simple electrospinning and carbonization process to prepare nitrogen-doped carbon nanofibres coupled with ZIF-8 metal-organic nanoparticles [32]. Nitrogen-doped carbon nanofibres were used as electrode modification materials. Then, we studied the electrochemical-sensing properties of nitrogen-doped carbon nanofibres for detecting Cd(II) and Pb(II) ions.

2. EXPERIMENTAL

Zinc nitrate hexahydrate, 2-methylimidazole, N-dimethylformamide (DMF), polyacrylonitrile (PAN), anhydrous sodium acetate, glacial acetic acid, isopropanol, and standard solutions of Cd(II) and Pb(II) were purchased from Macklin Co., Ltd. All chemicals were analytical-grade and used without purification. The working electrode, counter electrode and reference electrode were glassy carbon, Pt wire and Ag/AgCl (3 M), respectively. The electrochemical determination of metandienone was carried out using a CHI 1040C electrochemical workstation.

Preparation of ZIF-8: Five grams of zinc nitrate hexahydrate was dissolved in 250 mL methanol to prepare solution A. Then, 5 g of 2-methylimidazole was dissolved in 200 mL of methanol to prepare solution B. Solutions A and B were mixed and stirred rigorously for 5 min. After ageing at room temperature for 24 h, the precipitates obtained were washed by centrifugation at 8000 rpm. ZIF-8 nanoparticles were collected by washing with methanol and drying in an oven at 60 °C.

Preparation of ZIF-8/PAN nanofibres: ZIF-8 nanoparticles (0.5 g) were added to 10 mL DMF and sonicated for 30 min. Then, 0.4 g PAN was added to the above solution, and the mixture was continuously stirred for 12 h at room temperature. The working voltage of the electrospinning apparatus was 15 kV, and the high-pressure nozzle was placed at a distance of 30 cm from the aluminium foil. ZIF-8/PAN nanofibres were carbonized at 600 °C for 3 h in a N₂ atmosphere. The resulting material was then treated with 10% hydrochloric acid for 24 h to remove excess Zn. Finally, nitrogen-doped carbon nanofibres (N-Z-C) were dried in air at 80 °C.

Electrode modification: Five microlitres of N-Z-C was dip-coated onto a GCE and allowed to dry at ambient conditions. Then, 2 µL of Nafion (0.5 wt%) was dip-coated onto the N-Z-C/GCE and allowed to dry at ambient conditions.

3. RESULTS AND DISCUSSION

Figure 1 shows the schematic diagram of the stepwise preparation process of N-Z-C/GCE. ZIF-8 is a rhombic dodecahedron with an average size of 130 ± 10 nm. Due to its regular morphology and small size, ZIF-8 can be homogeneously dispersed in the electrospinning solution.

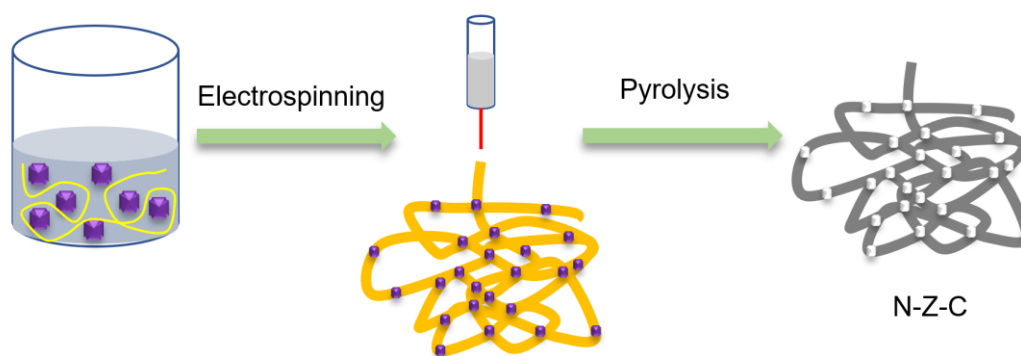


Figure 1. Schematic diagram of the stepwise preparation process of the N-Z-C/GCE.

To evaluate the specific surface area, structural defects and chemical structures of N-Z-C, we determined the specific surface area of N-Z-C by a nitrogen adsorption-desorption curve. Figure 2A shows the N₂ adsorption isotherm, which was similar to the characteristics of type IV. Obvious H3-hysteresis rings were observed, indicating that the nitrogen-doped carbon nanofibres had mesoporous structures. The specific surface area of the nitrogen-doped carbon nanofibres was approximately 161.4 m²/g, which indicated a higher number of active sites after nitrogen doping. The increase in the number

of active sites indicated more structural defects in N-Z-C, which suggested that a larger surface area and higher electrocatalytic activity of N-Z-C could be expected [33,34].

Figure 2B shows the Raman spectrum of the material, which confirmed the coexistence of D (1347 cm^{-1}) and G (1584 cm^{-1}) bands, in which the intensity ratio was 1.29 (I_D/I_G), indicating that the number of structural defects in nitrogen-doped carbon nanofibres was relatively high [35].

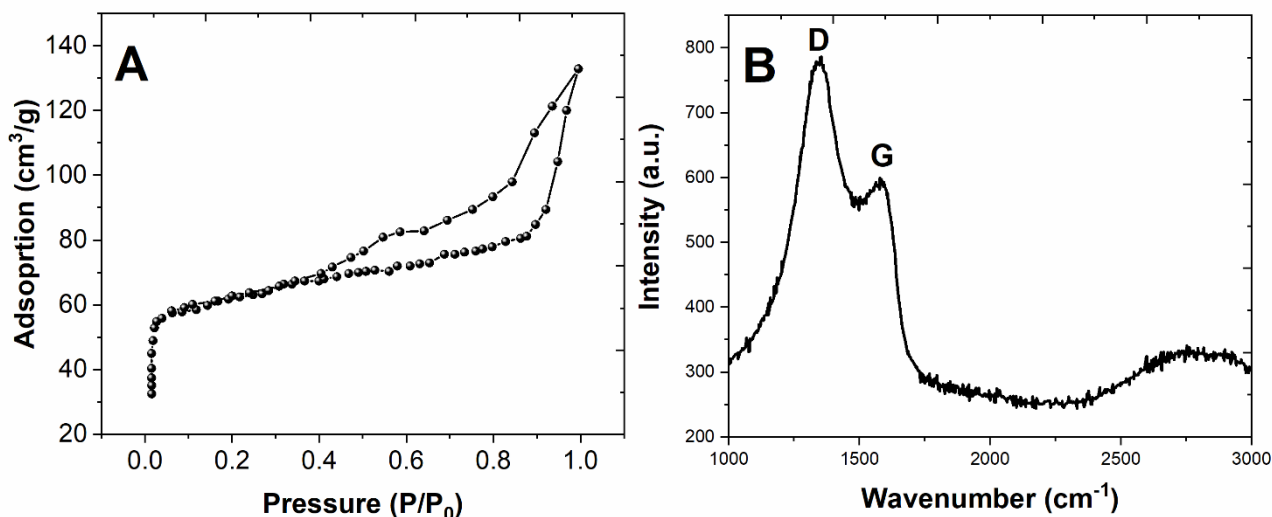


Figure 2. (A) Nitrogen sorption isotherms and (B) Raman spectrum of N-Z-C.

To more clearly evaluate the nitrogen composition of N-Z-C, XPS was used to characterize the materials. Figure 3A shows the XPS spectrum of the material, confirming the existence of C, N, O and residual Zn. The content of carbon was the highest, followed by nitrogen, and it was observed that the doping concentration of N in NCNFs was the lowest. This observation can be attributed to the low level of N-containing precursors in the material preparation process [36–40].

The high-resolution N_{1s} curve shows that the main peak of nitrogen appeared at 398.4 eV (Figure 3B), which can be deconvoluted into different peaks to characterize the chemical state of nitrogen. The main n-bond configurations are pyridine nitrogen at 398.2 eV, pyrrolidine nitrogen at 401 eV and graphite nitrogen at 401.6 eV.

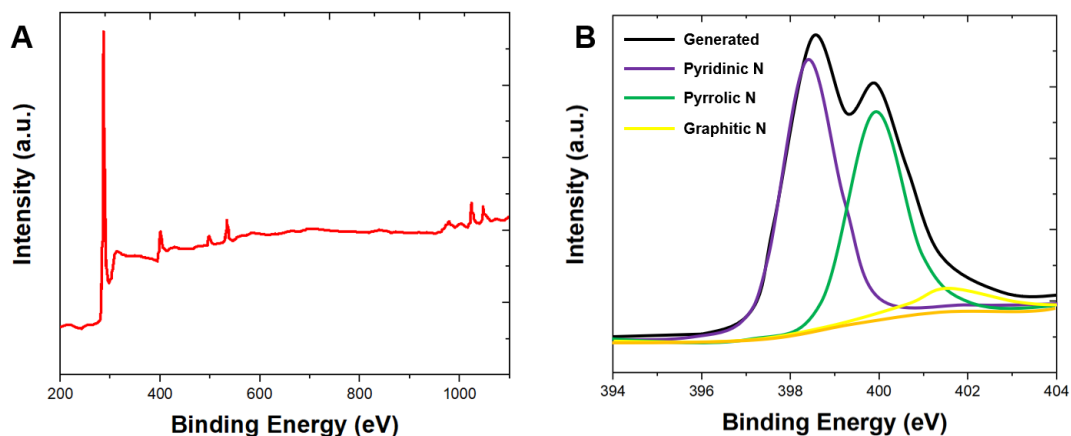


Figure 3. (A) Wide XPS spectrum and (B) high resolution N_{1s} spectrum of N-Z-C.

Anodic stripping voltammetry (ASV) is the main method to analyse the content of heavy metal ions, while differential pulse anodic stripping voltammetry (DPASV) is the main method to detect heavy metal elements. SWASV is mainly divided into three steps: accumulation, quiescence and dissolution [41]. The accumulation process refers to the measurement of the concentration potential of heavy metal ions in the solution, which is negative compared to the oxidation peak potential of heavy metal ions. During this process, heavy metal ions move towards the surface of the electrode, where they are reduced to metal atoms. As a result of this accumulation, the ions are enriched at the electrode surface [42]. This process only increases the Faraday current of the dissolution peak without increasing the charging current, which improves the response current of the electrochemical detection of heavy metals. Moreover, the presence of a modifier film on the electrode can further improve the electrode sensitivity because it could facilitate the preconcentration of metal cations at the electrode [43–48].

Bare GCE, Nafion-modified GCE and N-Z-C/GCE were used to study the response of different kinds of electrodes to Cd(II) and Pb(II). As shown in Figure 4, the response peak current of the bare GCE was $0.22 \mu\text{A}$ for Cd(II) and $0.55 \mu\text{A}$ for Pb(II). The electrochemical signals of Cd(II) and Pb(II) increased slightly when the Nafion/GCE was used. In contrast, the N-Z-C/GCE showed the best electrochemical sensing performance among the three electrodes. When comparing the results of the three electrodes, the sharp increase in the Cd(II) and Pb(II) peak currents on the N-Z-C/GCE is mainly attributed to the expansion of the surface area of the electroactive sites and the increase in the number of active sites [49,50]. At the same time, the pore structure reduces the resistance of heavy metal ions in the fibre. In addition, the higher N content in N-Z-C provides excellent affinity for Cd(II) and Pb(II) [51,52].

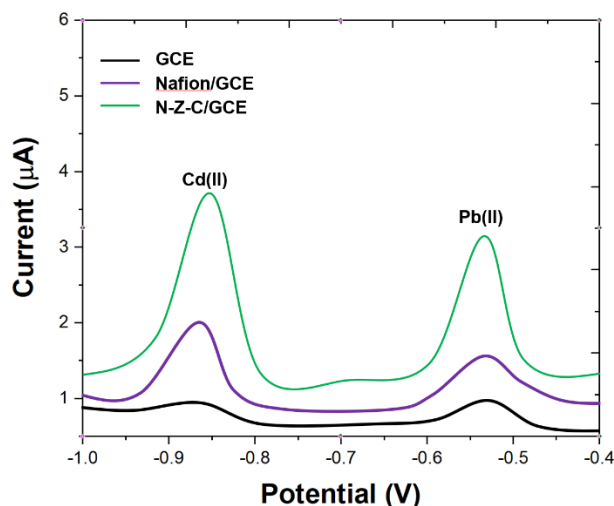


Figure 4. DPASV curves of bare GCE, naifion/GCE and N-Z-C/CGE in 0.1 M HAc-NaAc buffer (pH = 5.5) containing 50 $\mu\text{g/L}$ of Cd(II) and Pb(II).

The DPASV peak currents of Cd(II) and Pb(II) were affected by experimental parameters and conditions, such as the amount of N-Z-C deposition potential, accumulation time, accumulation potential and pH. We first studied the effect of the N-Z-C load on the sensor. The peak currents of Cd(II) and Pb(II) increased upon increasing the N-Z-C loading to 4 μg . When the load mass exceeded 4 μg , the response current decreased. This phenomenon can be attributed to the fact that a higher mass of N-Z-C results in thicker films on the electrode surface, which increases the pseudocapacitance and slows down the electron transfer at the interface of the electrode and the solution. Therefore, to optimize the detection, 4 μg of N-Z-C was selected.

The peak currents of Cd(II) and Pb(II) were also affected by the accumulation potential. Therefore, we studied the DPASV detection of Cd(II) and Pb(II) at varying accumulation potentials. The accumulation potential ranged from -1.4 V to -1.0 V, and the accumulation time was approximately 100 s. The peak currents of Cd(II) and Pb(II) increased with the decrease in the accumulation potential to -1.3 V. When the accumulation potential was higher than -1.3 V, the response current decreased, which indicated that the lower accumulation potential caused a significant hydrogen evolution reaction. More bubbles were generated on the surface of the electrode, thus preventing the effective accumulation of heavy metal ions on the surface of the modified electrode. Therefore, -1.3 V was selected as the optimal accumulation potential.

The accumulation time also affected the detection of Cd(II) and Pb(II). When the response current increased from 30 s to 100 s, the response currents of Cd(II) and Pb(II) also increased over time. This increase occurred because a longer accumulation time promotes the formation of Cd and Pb alloys. When the deposition time was longer than 100 s, the peak current of Cd(II) decreased slightly, while that of Pb(II) increased slowly. This behaviour can be attributed to the competitive adsorption of Cd(II) and Pb(II) when they form alloys. Therefore, 100 s was selected as the best accumulation time.

When the pH value was lower than 5.5, the peak currents of Cd(II) and Pb(II) increased with increasing pH. When the pH exceeded 5.5, the peak currents of Cd(II) and Pb(II) decreased sharply due to the hydrolysis of Cd(II) and Pb(II). Based on this result, pH = 5.5 was selected as the best pH value.

Under the optimal experimental parameters and conditions, the concentrations of Cd(II) and Pb(II) were determined by the N-Z-C/GCE. By employing the variable method, one analyte was kept at a constant concentration to measure another analyte. Figure 5A shows the DPASV of Cd(II) from 2 $\mu\text{g/L}$ to 100 $\mu\text{g/L}$ in the presence of 50 $\mu\text{g/L}$ Pb(II). A linear relationship was obtained with a limit of detection of 1.11 $\mu\text{g/L}$ (Figure 5B). Figure 6A shows the DPASV of Pd(II) from 1 $\mu\text{g/L}$ to 100 $\mu\text{g/L}$ in the presence of 50 $\mu\text{g/L}$ Cd(II). A linear relationship was obtained with a limit of detection of 0.72 $\mu\text{g/L}$ (Figure 6B). The data in Figure 5b and 6b were subtracted from the background. Therefore, the current values of the data points were lower than the peak value obtained in Figure 5a and 5b. To verify the superiority of N-Z-C in the detection of heavy metals, we compared the detection results published in recent years. As shown in Table 1, compared with other methods, the new method has a lower detection limit and a wider linear range.

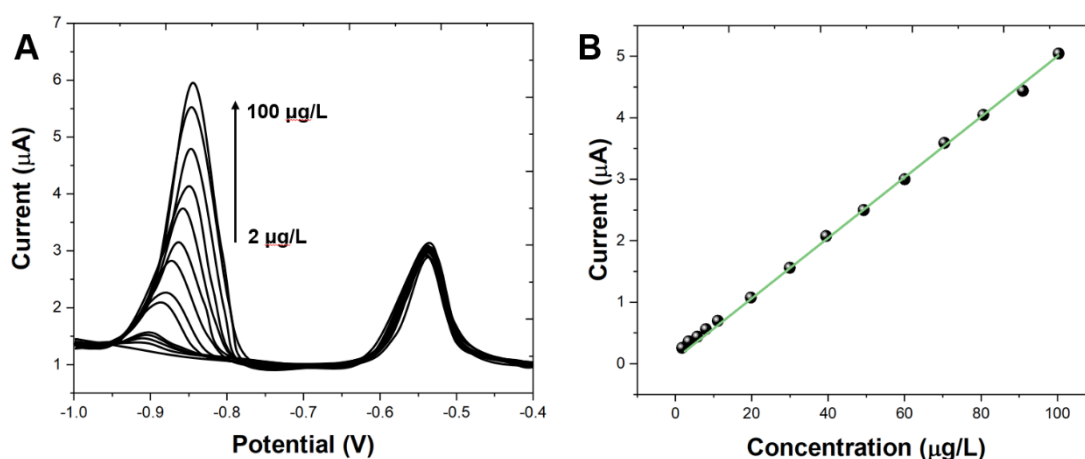


Figure 5. (A) DPASV curves of the N-Z-C/CGE in Cd(II) solution in the concentration from 2 $\mu\text{g/L}$ to 100 $\mu\text{g/L}$ in the presence of the 50 $\mu\text{g/L}$ of Pb(II). (B) Linear calibration plot of N-Z-C/CGE against the concentration of Cd(II).

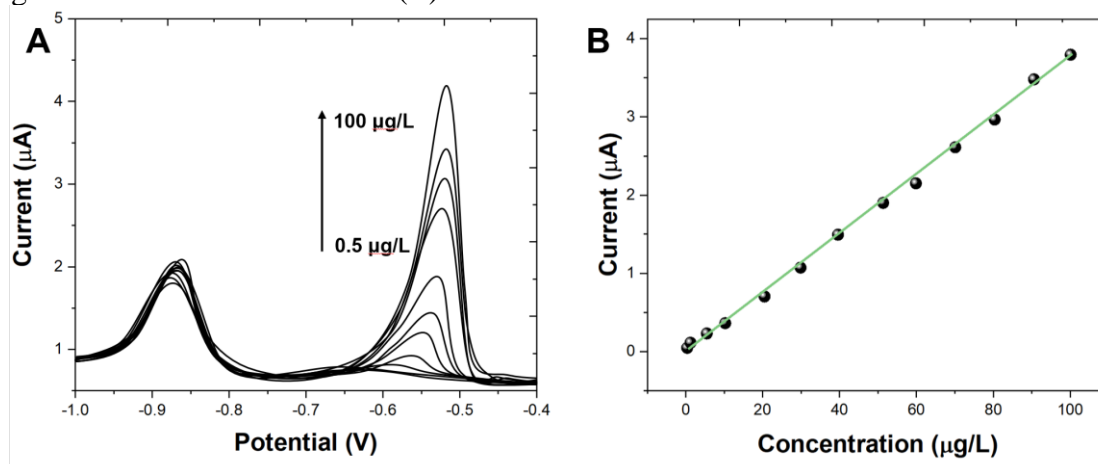
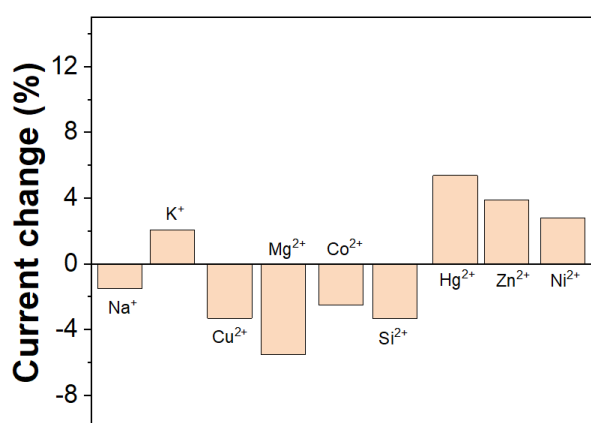


Figure 6. (A) DPASV curves of the N-Z-C/CGE in Pd(II) solution in the concentration from 1 $\mu\text{g/L}$ to 100 $\mu\text{g/L}$ in the presence of the 50 $\mu\text{g/L}$ of Cd(II). (B) Linear calibration plot of N-Z-C/CGE against the concentration of Pd(II).

Table 1. Comparison of Pd(II) and Cd(II) sensing using proposed method with previous reports.

Electrode	Linear of detection	Limit of Detection	Reference
AgNPr/Bi/Nafion	Cd(II): 10 $\mu\text{g/L}$ to 500 $\mu\text{g/L}$ Pd(II): 10 $\mu\text{g/L}$ to 500 $\mu\text{g/L}$	Cd(II): 4.4 $\mu\text{g/L}$ Pd(II): 3.3 $\mu\text{g/L}$	[53]
Bixerogel/Nafion/GCE	Cd(II): 0.6 $\mu\text{g/L}$ to 11.2 $\mu\text{g/L}$ Pd(II): 1 $\mu\text{g/L}$ to 20.7 $\mu\text{g/L}$	Cd(II): 0.4 $\mu\text{g/L}$ Pd(II): 1.3 $\mu\text{g/L}$	[54]
Nafion/Bi/NMC/GCE	Cd(II): 2 $\mu\text{g/L}$ to 100 $\mu\text{g/L}$ Pd(II): 0.5 $\mu\text{g/L}$ to 100 $\mu\text{g/L}$	Cd(II): 1.5 $\mu\text{g/L}$ Pd(II): 0.1 $\mu\text{g/L}$	[55]
Diatomite-MPTMS/GCE	Cd(II): 20 $\mu\text{g/L}$ to 300 $\mu\text{g/L}$ Pd(II): 20 $\mu\text{g/L}$ to 150 $\mu\text{g/L}$	Cd(II): 4.4 $\mu\text{g/L}$ Pd(II): 3.3 $\mu\text{g/L}$	[56]
N-Z-C/CGE	Cd(II): 2 $\mu\text{g/L}$ to 100 $\mu\text{g/L}$ Pd(II): 1 $\mu\text{g/L}$ to 100 $\mu\text{g/L}$	Cd(II): 1.11 $\mu\text{g/L}$ Pd(II): 0.72 $\mu\text{g/L}$	This work

To discuss the selectivity of N-Z-C/CGE, 9 common ions that may interfere with the actual detection of Cd(II) and Pd(II) were introduced in this experiment, as shown in Figure 7. The results showed that sodium ions, potassium ions, copper ions, manganese ions, cobalt ions, silicon ions, mercury ions, zinc ions and nickel ions did not interfere with the actual detection of Cd(II) and Pd(II), although their concentrations were 10 times higher than those of Cd(II) and Pd(II). Therefore, the proposed sensor exhibited excellent selectivity.

**Figure 7.** Anti-interference property of the N-Z-C/CGE.

The N-Z-C/CGE was also examined the real applicability for simultaneous determination of Cd(II) and Pd(II) in water from local river. As listed in Table 2, the acceptable average recoveries for

Cd(II) and Pd(II) are obtained (within 6% RSD), confirming that this proposal sensor can be used for simultaneous determination of Cd(II) and Pd(II) in real water samples.

Table 2. Simultaneous determination of Cd(II) and Pd(II) in real water samples by N-Z-C/CGE.

Sample	Added ($\mu\text{g/L}$)		Cd(II)			Pd(II)		
	Cd(II)	Pd(II)	Found	Recovery	RSD	Found	Recovery	RSD
River water	0	0	0	-	-	0	-	-
	20.00	20.00	19.79	98.95%	3.52%	20.27	101.35%	5.20%
	30.00	30.00	30.22	100.73%	5.12%	28.57	95.23%	4.58%

4. CONCLUSION

Nitrogen-doped carbon nanofibres were prepared by direct carbonization of ZIF-8/PAN electrospun nanofibres. The proposed N-Z-C can be used to prepare electrochemical sensors for the detection of Cd(II) and Pb(II) ions. Due to the porous structure, three-dimensional network structure and large number of nitrogen-doped defects, the N-Z-C/GCE exhibited enhanced electrochemical sensing properties for both Cd(II) and Pb(II). The DPASV current change of the target ions was less than 10% when 10 interfering substances were added, which indicates that N-Z-C can be used to monitor the heavy metal ions Cd(II) and Pb(II) in wastewater.

References

1. A. Shah, A. Nisar, K. Khan, J. Nisar, A. Niaz, M.N. Ashiq, M.S. Akhter, *Electrochimica Acta*, 321 (2019) 134658.
2. K. Kamde, R. Dahake, R. Pandey, A. Bansiwala, *Environ. Technol.*, 40 (2019) 1337–1348.
3. Q. Kong, Z. Li, Y. Zhao, C. Wei, G. Qiu, C. Wei, *J. Environ. Manage.*, 247 (2019) 234–241.
4. A. Adekunle, V. Raghavan, B. Tartakovsky, *Biosens. Bioelectron.*, 132 (2019) 382–390.
5. A.N. Berlina, A.V. Zherdev, B.B. Dzantiev, *Microchim. Acta*, 186 (2019) 1–39.
6. L. Yang, T. Wen, L. Wang, T. Miki, H. Bai, X. Lu, H. Yu, T. Nagasaka, *J. Environ. Manage.*, 231 (2019) 41–48.
7. L. Zhang, D. Peng, R.-P. Liang, J.-D. Qiu, *TrAC Trends Anal. Chem.*, 102 (2018) 280–289.
8. N. Can, B.C. Ömür, A. Altındal, *Sens. Actuators B Chem.*, 237 (2016) 953–961.
9. Y. Liu, Y. Deng, H. Dong, K. Liu, N. He, *Sci. China Chem.*, 60 (2017) 329–337.
10. T. Liu, Y. Wei, G. Song, B. Hu, L. Li, G. Jin, J. Wang, Y. Li, C. Song, Z. Shi, L. Zhao, J. Hu, W. Zhao, M. Hou, R. Li, J. Wang, *Measurement*, 124 (2018) 211–223.
11. L. Zhang, D. Peng, R.-P. Liang, J.-D. Qiu, *TrAC Trends Anal. Chem.*, 102 (2018) 280–289.
12. J. Jia, H. Li, S. Zong, B. Jiang, G. Li, O. Ejenavi, J. Zhu, D. Zhang, *Sens. Actuators B Chem.*, 222 (2016) 290–299.
13. Y. Zhang, Y. Sun, L. Cai, Y. Gao, Y. Cai, *Measurement*, 158 (2020) 107742.
14. H.R. Lotfi Zadeh Zhad, Y.M. Rodríguez Torres, R.Y. Lai, *J. Electroanal. Chem.*, 803 (2017) 89–94.
15. J. Han, J. Yu, Y. Guo, L. Wang, Y. Song, *Sens. Actuators B Chem.*, 321 (2020) 128498.

16. X.-M. Bi, H.-R. Wang, L.-Q. Ge, D.-M. Zhou, J.-Z. Xu, H.-Y. Gu, N. Bao, *Sens. Actuators B Chem.*, 260 (2018) 475–479.
17. S. Kempahanumakkagari, A. Deep, K.-H. Kim, S. Kumar Kailasa, H.-O. Yoon, *Biosens. Bioelectron.*, 95 (2017) 106–116.
18. D. Martín-Yerga, I. Álvarez-Martos, M.C. Blanco-López, C.S. Henry, M.T. Fernández-Abedul, *Anal. Chim. Acta*, 981 (2017) 24–33.
19. Z. Liu, E. Puumala, A. Chen, *Sens. Actuators B Chem.*, 287 (2019) 517–525.
20. M. Malakootian, S. Hamzeh, H. Mahmoudi-Moghaddam, *Microchem. J.*, 158 (2020) 105194.
21. Y.-F. Sun, Jian-Wang, P.-H. Li, M. Yang, X.-J. Huang, *Sens. Actuators B Chem.*, 292 (2019) 136–147.
22. X. Lin, Z. Lu, W. Dai, B. Liu, Y. Zhang, J. Li, J. Ye, *J. Electroanal. Chem.*, 828 (2018) 41–49.
23. L. Fu, K. Xie, A. Wang, F. Lyu, J. Ge, L. Zhang, H. Zhang, W. Su, Y.-L. Hou, C. Zhou, *Anal. Chim. Acta*, 1081 (2019) 51–58.
24. L. Fu, Y. Zheng, P. Zhang, H. Zhang, Y. Xu, J. Zhou, H. Zhang, H. Karimi-Maleh, G. Lai, S. Zhao, W. Su, J. Yu, C.-T. Lin, *Biosens. Bioelectron.*, 159 (2020) 112212.
25. L. Fu, Y. Zheng, P. Zhang, H. Zhang, M. Wu, H. Zhang, A. Wang, W. Su, F. Chen, J. Yu, W. Cai, C.-T. Lin, *Bioelectrochemistry*, 129 (2019) 199–205.
26. P.-H. Li, Y.-X. Li, S.-H. Chen, S.-S. Li, M. Jiang, Z. Guo, J.-H. Liu, X.-J. Huang, M. Yang, *Sens. Actuators B Chem.*, 257 (2018) 1009–1020.
27. M.B. Gumpu, M. Veerapandian, U.M. Krishnan, J.B.B. Rayappan, *Talanta*, 162 (2017) 574–582.
28. S.A. Kitte, S. Li, A. Nsabimana, W. Gao, J. Lai, Z. Liu, G. Xu, *Talanta*, 191 (2019) 485–490.
29. S. Deshmukh, G. Kandasamy, R.K. Upadhyay, G. Bhattacharya, D. Banerjee, D. Maity, M.A. Deshusses, S.S. Roy, *J. Electroanal. Chem.*, 788 (2017) 91–98.
30. X. Li, H. Zhou, C. Fu, F. Wang, Y. Ding, Y. Kuang, *Sens. Actuators B Chem.*, 236 (2016) 144–152.
31. L. Xiao, B. Wang, L. Ji, F. Wang, Q. Yuan, G. Hu, A. Dong, W. Gan, *Electrochimica Acta*, 222 (2016) 1371–1377.
32. D. Qin, A. Chen, X. Mamat, Y. Li, X. Hu, P. Wang, H. Cheng, Y. Dong, G. Hu, *Anal. Chim. Acta*, 1078 (2019) 32–41.
33. Y. Li, Y. Zhao, H. Cheng, Y. Hu, G. Shi, L. Dai, L. Qu, *J. Am. Chem. Soc.*, 134 (2012) 15–18.
34. L. Li, D. Liu, K. Wang, H. Mao, T. You, *Sens. Actuators B Chem.*, 252 (2017) 17–23.
35. X. Wu, S. Wu, Y. Li, H. Chen, Q. Yuan, W. Gan, *Anal. Chim. Acta*, 1046 (2019) 115–122.
36. X. Zhang, D. Liu, B. Yu, T. You, *Sens. Actuators B Chem.*, 224 (2016) 103–109.
37. Z. Shamsadin-Azad, M.A. Taher, S. Cheraghi, H. Karimi-Maleh, *J. Food Meas. Charact.*, 13 (2019) 1781–1787.
38. H. Karimi-Maleh, F. Karimi, S. Malekmohammadi, N. Zakariae, R. Esmaeili, S. Rostamnia, M.L. Yola, N. Atar, S. Movagharnezhad, S. Rajendran, *J. Mol. Liq.* (2020) 113185.
39. L. Fu, Z. Liu, J. Ge, M. Guo, H. Zhang, F. Chen, W. Su, A. Yu, *J. Electroanal. Chem.*, 841 (2019) 142–147.
40. J. Zhou, M. Wu, Y. Xu, Z. Li, Y. Yao, L. Fu, *Int J Electrochem Sci*, 15 (2020) 5793–5802.
41. X. Zhu, B. Liu, H. Hou, Z. Huang, K.M. Zeinu, L. Huang, X. Yuan, D. Guo, J. Hu, J. Yang, *Electrochimica Acta*, 248 (2017) 46–57.
42. H. Xing, J. Xu, X. Zhu, X. Duan, L. Lu, W. Wang, Y. Zhang, T. Yang, *J. Electroanal. Chem.*, 760 (2016) 52–58.
43. M. Zhang, B. Pan, Y. Wang, X. Du, L. Fu, Y. Zheng, F. Chen, W. Wu, Q. Zhou, S. Ding, *ChemistrySelect*, 5 (2020) 5035–5040.
44. J. Ying, Y. Zheng, H. Zhang, L. Fu, *Rev. Mex. Ing. Quím.*, 19 (2020) 585–592.
45. L. Fu, Q. Wang, M. Zhang, Y. Zheng, M. Wu, Z. Lan, J. Pu, H. Zhang, F. Chen, W. Su, *Front. Chem.*, 8 (2020) 92.

46. H. Karimi-Maleh, K. Cellat, K. Arıkan, A. Savk, F. Karimi, F. Şen, *Mater. Chem. Phys.* (2020) 123042.
47. H. Karimi-Maleh, O.A. Arotiba, *J. Colloid Interface Sci.*, 560 (2020) 208–212.
48. N. Ruecha, N. Rodthongkum, D.M. Cate, J. Volckens, O. Chailapakul, C.S. Henry, *Anal. Chim. Acta*, 874 (2015) 40–48.
49. Z. Guo, M.-L. Seol, C. Gao, M.-S. Kim, J.-H. Ahn, Y.-K. Choi, X.-J. Huang, *Electrochimica Acta*, 211 (2016) 998–1005.
50. Y. Wu, T. Yang, K.-C. Chou, J. Chen, L. Su, X. Hou, *Analyst*, 142 (2017) 2741–2747.
51. X. Qin, D. Tang, Y. Zhang, Y. Cheng, F. He, Z. Su, H. Jiang, *Int J Electrochem Sci*, 15 (2020) 1517–1528.
52. T. Jackfama, M. Moyo, T. Nharingo, M. Shumba, J. Okonkwo, *Int. J. Environ. Anal. Chem.*, 99 (2019) 47–60.
53. N. Promphet, P. Rattanarat, R. Rangkupan, O. Chailapakul, N. Rodthongkum, *Sens. Actuators B Chem.*, 207 (2015) 526–534.
54. P.A. Dimovasilis, M.I. Prodromidis, *Anal. Chim. Acta*, 769 (2013) 49–55.
55. L. Xiao, H. Xu, S. Zhou, T. Song, H. Wang, S. Li, W. Gan, Q. Yuan, *Electrochimica Acta*, 143 (2014) 143–151.
56. D. Quang Khieu, B.H. Dang Son, V. Thi Thanh Chau, P. Dinh Du, N. Hai Phong, N. Thi Diem Chau, *J. Chem.*, 2017 (2017) 1–10.

© 2020 The Authors. Published by ESG (www.electrochemsci.org). This article is an open access article distributed under the terms and conditions of the Creative Commons Attribution license (<http://creativecommons.org/licenses/by/4.0/>).